$^{64}CuCl_2$ PET/CT in Prostate Cancer Relapse

Arnoldo Piccardo[1], Francesco Paparo[2], Matteo Puntoni[3], Sergio Righi[4], Gianluca Bottoni[1], Lorenzo Bacigalupo[2], Silvia Zanardi[5], Andrea DeCensi[5], Giulia Ferrarazzo[1], Monica Gambaro[4], Filippo Grillo Ruggieri[6], Fabio Campodonico[7], Laura Tomasello[8], Luca Timossi[9], Simona Sola[10], Egesta Lopci*[11], and Manlio Cabria*[1]

[1]Department of Nuclear Medicine, Galliera Hospital, Genoa, Italy; [2]Department of Radiology, E.O. Galliera Hospital, Genoa, Italy; [3]Clinical Trial Unit, Office of the Scientific Director, Galliera Hospital, Genoa, Italy; [4]Medical Physics Department, E.O. Galliera Hospital, Genoa, Italy; [5]Department of Oncology, E.O. Galliera Hospital, Genoa, Italy; [6]Department of Radiotherapy, E.O. Galliera Hospital, Genoa, Italy; [7]Department of Urology, E.O. Galliera Hospital, Genoa, Italy; [8]Department of Oncology, IRCCS San Martino IST, University of Genoa, Genoa, Italy; [9]Department of Urology, E.O. Evangelico Internazionale Hospital, Genoa, Italy; [10]Department of Histopathology, E.O. Galliera Hospital, Genoa, Italy; and [11]Department of Nuclear Medicine, Humanitas Research Hospital, Milano, Italy

See an invited perspective on this article on page 442.

Our objective was to evaluate the biodistribution, kinetics, and radiation dosimetry of $^{64}CuCl_2$ in humans and to assess the ability of $^{64}CuCl_2$ PET/CT to detect prostate cancer (PCa) recurrence in patients with biochemical relapse. **Methods:** We prospectively evaluated 50 PCa patients with biochemical relapse after surgery or external-beam radiation therapy. All patients underwent $^{64}CuCl_2$ PET/CT, ^{18}F-choline PET/CT, and multiparametric MRI within 15 d of each other. Experienced readers interpreted the images, and the detection rate (DR) of each imaging modality was calculated. Histopathology, when available; clinical or laboratory response; and multidisciplinary follow-up were used to confirm the site of disease. In parallel, biodistribution, kinetics of the lesions, and radiation dosimetry of $^{64}CuCl_2$ were evaluated. **Results:** From a dosimetric point of view, an administered dose of 200 MBq for $^{64}CuCl_2$ translated into a 5.7-mSv effective dose. Unlike ^{18}F-choline, $^{64}CuCl_2$ was not excreted or accumulated in the urinary tract, thus allowing thorough pelvic exploration. The maximum $^{64}CuCl_2$ uptake at the sites of PCa relapse was observed 1 h after tracer injection. In our cohort, $^{64}CuCl_2$ PET/CT proved positive in 41 of 50 patients, with an overall DR of 82%. The DRs of ^{18}F-choline PET/CT and multiparametric MRI were 56% and 74%, respectively. The difference between the DRs of $^{64}CuCl_2$ PET/CT and ^{18}F-choline PET/CT was statistically significant ($P < 0.001$). Interestingly, on considering prostate-specific antigen (PSA) value, $^{64}CuCl_2$ PET/CT had a higher DR than ^{18}F-choline PET/CT in patients with a PSA of less than 1 ng/mL. **Conclusion:** The biodistribution of $^{64}CuCl_2$ is more suitable than that of ^{18}F-choline for exploring the pelvis and prostatic bed. The $^{64}CuCl_2$ effective dose is like those of other established PET tracers. In patients with biochemical relapse and a low PSA level, $^{64}CuCl_2$ PET/CT shows a significantly higher DR than ^{18}F-choline PET/CT.

Key Words: prostate cancer; $^{64}CuCl_2$; dosimetry; elderly; PET/CT

J Nucl Med 2018; 59:444–451
DOI: 10.2967/jnumed.117.195628

Received May 11, 2017; revision accepted Jul. 25, 2017.
For correspondence or reprints contact: Arnoldo Piccardo, Department of Nuclear Medicine, E.O. Ospedali Galliera, Mura delle Cappuccine 14, 16128 Genoa, Italy.
E-mail: arnoldo.piccardo@galliera.it
*Contributed equally to this work.
Published online Sep. 8, 2017.

Copper is a chemical element required for the normal functioning of many molecules involved in the signal transduction pathway regulating cell proliferation. It plays an important role in tumor angiogenesis (*1–3*) and can stimulate endothelial cell proliferation (*4*). So far, we know that copper metabolism and its cellular deposition are altered in neoplastic disease (*5*). Several authors have reported an increased copper content in tumors (*6,7*), giving rise to the possibility of using elevated copper concentration in cancer cells as an imaging biomarker for metabolic PET imaging (*8,9*). Human copper transporter 1 is a high-affinity copper transporter that mediates cellular uptake of copper in humans (*10*). This transporter is well represented in human cancer, including prostate tumor cells. Preclinical studies have shown that human prostate cancer (PCa) xenograft models in mice display an increased uptake of copper administered as $^{64}CuCl_2$ (*10,11*). So far, only one paper, involving few patients, has confirmed the ability of $^{64}CuCl_2$ PET/CT to detect PCa sites of disease in humans (*12*). To the best of our knowledge, no studies have assessed the ability of $^{64}CuCl_2$ PET/CT to detect PCa relapse after surgery or external-beam radiation therapy (EBRT).

Whereas ^{18}F-choline and ^{11}C-choline remain the most validated tracers for the detection of recurrent PCa (*13,14*), they have significant limitations in terms of sensitivity in the case of low prostate-specific antigen (PSA) level and long PSA doubling time (*15*). In this field, the recent introduction of new PET radiopharmaceuticals (e.g., ^{68}Ga-PSMA and ^{18}F-FACBC) (*16–19*), and the possibility of obtaining PET/MRI using dedicated software (*20,21*) or dedicated tomographs (*22*), have increased sensitivity in the early detection of PCa relapse, especially in the case of low PSA levels.

In the current trial we aimed to evaluate, for the first time, the ability of $^{64}CuCl_2$ PET/CT to detect PCa recurrence in patients presenting with biochemical relapse. We compared all the above-mentioned results with those of ^{18}F-choline PET/CT and multiparametric MRI (mpMRI). We also aimed to assess the clinical safety, biodistribution, and radiation dosimetry of $^{64}CuCl_2$ in humans. Moreover, we studied the $^{64}CuCl_2$ kinetics of sites of PCa relapse.

MATERIALS AND METHODS

The local ethics committee and the "Agenzia Italiana del Farmaco," a public agency of the Italian Ministry of Health, approved this study. All subjects signed a written informed consent form. The trial was

TABLE 1
Patient Characteristics

Characteristic	Data
Median age (y)	72 (range, 52–90)
PSA level (ng/mL)	
Mean	3.26 (SD, 3.06)
Median	1.88 (range, 0.24–14.0)
Median PSA doubling time (mo)	4.2 (range, 0.9–34.0)
Median PSA velocity (ng/mL/y)	2.0 (range, 0.1–56.4)
Gleason score (*n*)	
3 + 4	12 (24%)
4 + 3	16 (32%)
4 + 4	17 (34%)
4 + 5	1 (2%)
5 + 4	4 (8%)
Treatment at time of biochemical relapse (*n*)	
Radical prostatectomy only	14 (28%)
Radical intent EBRT only	8 (16%)
Hormone therapy only	3 (6%)
Radical prostatectomy + salvage EBRT	8 (16%)
Radical prostatectomy + hormone therapy	4 (8%)
Radical prostatectomy + EBRT + hormone therapy	7 (14%)
Radical intent EBRT + hormone therapy	6 (12%)

registered in the European Clinical Trial Database (EudraCT number 2014-005140-18).

Patient Population

From February to October 2016, we prospectively evaluated 50 PCa patients presenting with biochemical relapse (*23*) after first-line surgery or EBRT. We also included patients with rising PSA levels after salvage EBRT or hormone therapy. All patients underwent $^{64}CuCl_2$ PET/CT, ^{18}F-choline PET/CT, and mpMRI within 15 d of one another. Table 1 shows the main characteristics of patients and tumors.

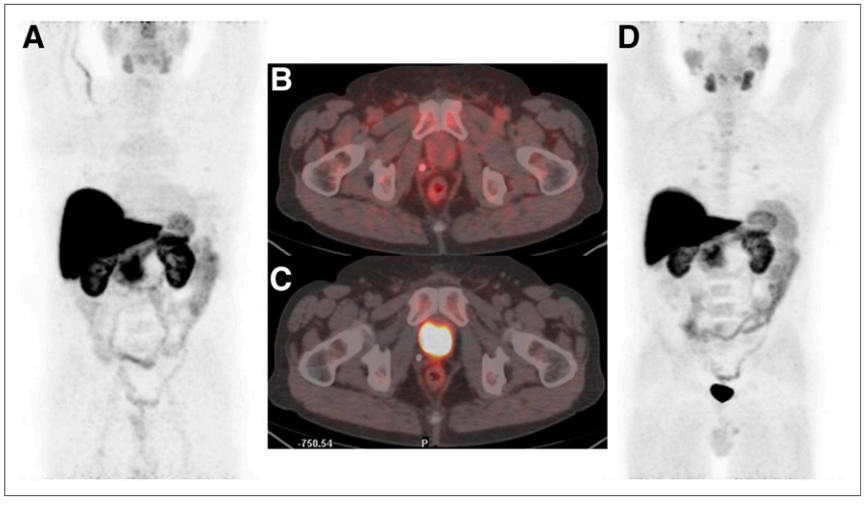

FIGURE 1. Maximum-intensity-projection images and PET/CT images of pelvis when $^{64}CuCl_2$ (A and B) and ^{18}F-choline (C and D) were used. Images were acquired 1 h and 20 min after $^{64}CuCl_2$ and ^{18}F-choline injection, respectively.

$^{64}CuCl_2$ PET/CT

The production of the experimental $^{64}CuCl_2$ (Sparkle s.r.l.) was approved by Agenzia Italiana del Farmaco. The radiopharmaceutical was prepared in accordance with good manufacturing practices and administered intravenously to fasting patients (≥6 h). Whole-body $^{64}CuCl_2$ PET/CT was performed 60 min (*12*) after injection of 200–250 MBq of $^{64}CuCl_2$. PET scans were acquired in 3-dimensional mode by a PET/CT system (Discovery ST; GE Healthcare). Considering the relatively low positron production and 511-keV photon emission (yield) of ^{64}Cu when compared with those of ^{18}F, PET/CT scans were acquired via 6-min emissions per bed position from the upper neck to the upper thighs, by means of sequential fields of view, each covering 12 cm (matrix of 256 × 256). Images were visualized on a Xeleris Workstation, version 2.1753 (GE Healthcare).

Low-dose CT was performed for both attenuation correction and topographic localization. The CT parameters used for acquisition were 140 kV, 80 mA, and 0.5 s per rotation, with a pitch of 6:1 and a slice thickness of 3.25 mm.

To evaluate the biodistribution and dosimetry of this radiopharmaceutical, all 50 patients underwent another 2 PET/CT acquisitions 4 h and 24 h after tracer injection. The second acquisition time (4 h) was selected in order to have a late acquisition on the same day as the tracer injection to facilitate patient compliance. The third acquisition time (24 h) was selected in order to have a late PET/CT acquisition (after 2 half-lives of the tracer) to improve the quality of the kinetics study.

TABLE 2
Absorbed Organ Dose per Administered Activity: Comparison with ^{18}F-Choline and ^{68}Ga-PSMA (*39*)

Organ	^{64}CuCl	^{18}F-choline	^{68}Ga-PSMA
Adrenals	2.56E–02	2.00E–02	1.42E–02
Brain	1.09E–02	8.70E–03	9.00E–03
Breasts	1.27E–02	9.00E–03	8.80E–03
Gallbladder wall	7.84E–02	2.10E–02	1.44E–02
Lower larger intestine wall	1.29E–02	1.20E–02	1.23E–02
Upper large intestine wall	1.83E–02	1.40E–02	5.40E–02
Small intestine	1.66E–02	1.30E–02	1.63E–02
Stomach wall	1.76E–02	1.30E–02	1.20E–02
Heart wall	1.85E–02	2.00E–02	1.09E–02
Kidneys	1.39E–01	9.70E–02	2.62E–01
Liver	2.71E–01	6.10E–02	3.09E–02
Lungs	1.68E–02	1.70E–02	1.02E–02
Muscle	1.38E–02	1.10E–02	1.05E–02
Pancreas	8.39E–02	1.70E–02	1.38E–02
Red marrow	1.29E–02	1.30E–02	9.20E–03
Osteogenic cells	2.58E–02	—	1.42E–02
Skin	1.14E–02	8.00E–03	8.85E–02
Spleen	3.63E–02	3.60E–02	4.46E–02
Testes	1.15E–02	9.80E–03	1.04E–02
Thymus	1.36E–02	1.10E–02	9.90E–03
Thyroid	1.21E–02	1.10E–02	9.70E–03
Urinary bladder wall	1.33E–02	5.90E–02	1.30E–01
Salivary glands	3.70E–02	—	—
Total body	2.11E–02	—	—
Effective dose ICRP 60 (mSv/MBq)	3.02E–02	—	—
Effective dose ICRP 103 (mSv/MBq)	2.83E–02	2.00E–02	2.36E–02

To evaluate the potential hepatic radiotoxicity of $^{64}CuCl_2$ administration, according to Agenzia Italiana del Farmaco suggestions, blood tests were performed on all patients and used to determine the following parameters: hematocrit, hemoglobin, C-reactive protein, aspartate transaminase, alanine transaminase, alkaline phosphatase, albumin, total bilirubin, γ-glutamyl transferase, lactate dehydrogenase, total proteins, serum creatinine, and azotemia. The tests were performed immediately before radiopharmaceutical administration and 10 d after the first $^{64}CuCl_2$ whole-body scan.

^{18}F-Choline PET/CT

^{18}F-choline PET/CT was performed in the fasting state (≥6 h). An ^{18}F-choline activity of 200 MBq (IASOcholine; IASON Labormedizin GesmbH und Co. KG) was administered intravenously; data were acquired 20 min after the injection by means of the above-mentioned PET/CT system. PET was performed over an acquisition time of 3 min in the same manner as for $^{64}CuCl_2$ PET/CT and visualized on the same workstation. The same CT parameters were also used.

TABLE 3
Patient-Based Analysis

Site of disease	$^{64}CuCl_2$ PET/CT	^{18}F-choline PET/CT	*P**	mpMRI	*P**
All positive patients	41/50 (82%) (69–91)	28/50 (56%) (41–70)	<0.001	37/50 (74%) (60–85)	0.3
Local	32/50 (64%) (49–77)	15/50 (30%) (18–45)	<0.001	25/50 (50%) (36–64)	0.07
Lymph node	16/50 (32%) (20–47)	15/50 (30%) (18–45)	1.0	14/50 (28%) (16–43)	0.6
Bone	4/50 (8%) (2–19)	4/50 (8%) (2–19)	1.0	5/50 (10%) (3–22)	1.0

*McNemar test vs. $^{64}CuCl_2$ PET/CT.
Data are DR followed by percentage and 95% confidence interval for each diagnostic modality at each site of disease.

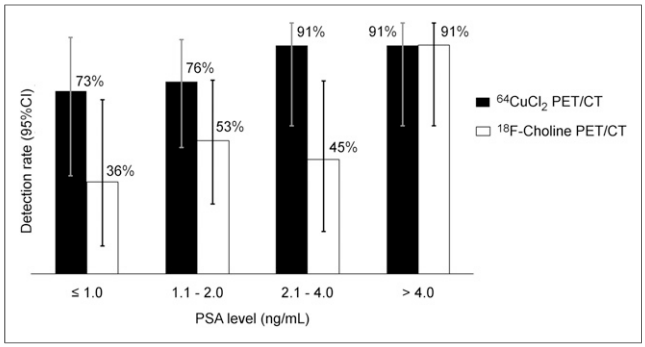

FIGURE 2. Patient-based analysis. Comparison of $^{64}CuCl_2$ PET/CT vs.^{18}F-choline PET/CT. DR was calculated for each PSA cohort.

mpMRI

All patients underwent mpMRI performed with a 1.5-T MRI scanner (Signa HDxt; GE Healthcare) equipped with an 8-channel pelvic phased-array surface coil. The procedure was performed according to a standardized protocol (*20*). A large–field-of-view fast spin echo T2-weighted sequence was set in order to visualize the pelvis and infrarenal paracaval and paraaortic lymph node stations. High-resolution oblique axial and coronal scans were further oriented perpendicular and parallel to the rectoprostatic plane. Diffusion-weighted imaging was acquired in the axial plane, using the same slice locations as for the first fast spin echo T2-weighted sequence. Dynamic contrast-enhanced MRI was acquired during intravenous injection of the paramagnetic contrast medium with a flow rate of 3 mL/s. A 3-dimensional spoiled gradient echo fat-saturated T1-weighted pulse sequence was repeated in the axial plane 27 times with a temporal resolution of 12 s, during the injection of a single dose of contrast agent. An axial short T1 inversion recovery sequence was performed to detect focal bone lesions.

Image Interpretation

All PET images were reviewed by 2 experienced nuclear medicine physicians (at least 5 y of experience in PET/CT examinations) masked to other PET/CT and mpMRI results. On ^{18}F-choline PET/CT and $^{64}CuCl_2$ PET/CT, any focal, nonphysiologic uptake higher than that of the surrounding background level was considered pathologic. The reference tissues were the prostate parenchyma, prostatic fossa, residual seminal vesicles, vesicourethral anastomoses, abdominal and pelvic lymph nodes, and bone.

^{18}F-choline PET/CT and $^{64}CuCl_2$ PET/CT studies were interpreted visually and semiquantitatively using the SUV_{max}, on a patient-by-patient and lesion-by-lesion basis. In patient-based analysis, detection rate (DR) was defined as the ability to detect at least one pathologic finding in each subject. In lesion-based analysis, the DR was defined as the ability to detect suspected lesions in relation to the total number of lesions detected by both tracers and mpMRI (*17*).

Tumor-to-background ratios (TBRs) were determined for each lesion on both the $^{64}CuCl_2$ and the ^{18}F-choline images. TBR was established by placing a 2-dimensional region of interest in the pelvis and measuring the SUV_{max} of the background fat within the area (*16*). This value was then used as the denominator for the TBR. No SUV_{max} or TBR cutoffs were introduced to assess tumor lesions, although these parameters were calculated as a support to visual interpretation.

All mpMRI studies were reviewed on a dedicated workstation (Advantage Workstation, version 4.6; GE Healthcare) by an abdominal radiologist (with at least 5 y of experience in prostate mpMRI) masked to the results of the PET studies.

PCa recurrence was diagnosed when a focal morphologic alteration was accompanied by at least one corresponding functional abnormality (on apparent-diffusion-coefficient or perfusion maps) or when 2 functional mpMRI criteria were present without a definite morphologic lesion. Morphologic criteria were also adopted to distinguish between benign and malignant lymph nodes (i.e., short-axis diameter $>$ 10 mm) (*20,21*). The axial short T1 inversion recovery sequence was used to detect bone metastases.

Standard of Reference

Although only DRs were calculated for each diagnostic modality, we applied a standard of reference, which could provide some confirmation of the site of disease. Histopathology was performed on transrectal ultrasound–guided biopsy in 7 of 25 patients (28%) showing only local recurrence; this confirmed the presence of disease. Moreover, undetectable PSA values were found after salvage EBRT in another 4 of the 11 patients with only local recurrence and not previously treated with EBRT. For lymph node and distant metastases, we used a multidisciplinary follow-up based on mpMRI, ^{18}F-choline PET/CT, and reduction of PSA values after salvage therapy. A median follow-up time of 7 mo (range, 5–15 mo) was available for each patient.

Radiation Dosimetry

For dosimetric calculation, volumes of interest were drawn, for all PET and CT datasets, using automatic rigid coregistration (PMOD). Time–activity curves for all organs and for the total body were fitted as a biexponential function. We calculated accumulated activity for each organ (the sum of all nuclear transitions inside the organ) as the area under the time–activity curve, and the residence time was obtained by dividing accumulated activity by administered activity. The accumulated activity of the remainder of the body was calculated by subtracting all source organs from the total-body activity. The absorbed dose for each organ was calculated using the MIRD system (*24,25*). S factors specific for a reference adult male for ^{64}Cu are tabulated in OLINDA/EXM software (*26*). The effective dose was

TABLE 4
Lesion-Based Analysis

Site of disease	$^{64}CuCl_2$ PET/CT	^{18}F-choline PET/CT	*P**	mpMRI	*P**
Local	40/44 (91%) (78–97)	15/44 (34%) (20–50)	<0.001	29/44 (66%) (50–80)	0.02
Lymph node	54/60 (90%) (79–96)	45/60 (75%) (62–85)	0.02	41/60 (68%) (55–80)	0.01
Bone	9/14 (64%) (35–87)	9/14 (64%) (35–87)	1.0	14/14 (100%) (77–100)†	0.06
All lesions	103/118 (87%) (80–93)	69/118 (59%) (49–67)	<0.001	84/118 (71%) (62–79)	0.007

*McNemar test vs. $^{64}CuCl_2$ PET/CT.
†One-sided, 97.5% confidence interval.
Data are DR followed by percentage and 95% confidence interval for each diagnostic modality at each site of disease.

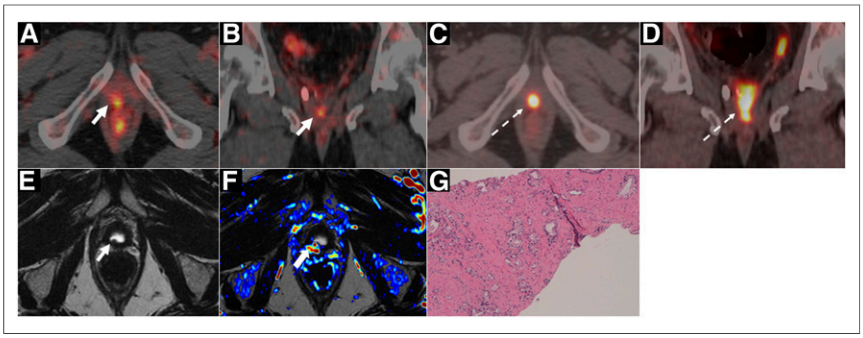

FIGURE 3. A 72-y-old man with Gleason 4 + 3 PCa treated with radical prostatectomy, with rising PSA level (1.0) and PSA doubling time of 11 mo. (A and B) $^{64}CuCl_2$ PET/CT images (axial and coronal) reveals focal tracer uptake (arrow) in vesicourethral anastomosis. (C and D) In ^{18}F-choline PET/CT images (axial and coronal), urinary tracer accumulation (dotted arrows) obscures walls of anastomosis. (E) T2-weighted mpMR image shows small hypointense nodular thickening (arrow) in anastomosis. (F) Wash-in perfusion map (derived from dynamic contrast-enhanced sequences) shows focal area of hypervascularization in correspondence to hypointense nodular thickening of anastomosis. (G) Local PCa relapse was histopathologically confirmed by transrectal ultrasound–guided biopsy (hematoxylin–eosin, ×10).

also calculated using the coefficients of radiosensitivity of the organs present in publications 60 and 103 of ICRP (*27,28*).

Lesion Kinetics

To evaluate lesion kinetics, volumes of interest were drawn for all PET and CT datasets using automatic rigid coregistration (PMOD). Time–activity curves for various lesions (all local-relapse lymph-node metastases with short axis diameter > 15 mm and all bones metastases) were fitted as a biexponential function to calculate maximum specific uptake and clearance.

Statistical Methods

Since no literature data were available on the experimental diagnostic method used, no formal test hypothesis or sample size calculation was made; therefore, the study was intended as a pilot, and sample size (n = 50) was determined on the basis of feasibility. The primary objective was to calculate and compare the DRs of the experimental tests ($^{64}CuCl_2$ PET/CT) with those of the standard tests (^{18}F-choline PET/CT and mpMRI).

The main descriptive statistics used were median, minimum, and maximum for continuous data and absolute and relative frequency for categoric data. DRs were calculated as the ratio between the number of positive patients (or lesions in the case of lesion-based analysis) and the total number of patients enrolled (or lesions). The exact binomial 95% confidence intervals of the DRs were calculated. The χ^2 and Fisher exact tests were adopted to compare categoric data; the exact McNemar test was used to compare DRs between diagnostic procedures on the same subjects, also stratified by total PSA levels (<1, 1.1–2, 2.1–4, and >4 ng/mL). A 2-tailed, paired test was used to analyze and compare TBR ratios between scans. Because the study was exploratory, no corrections for multiple tests were applied. Statistical significance was assigned to values of α-error (2-tailed) lower than 0.05. All statistical analyses used Stata software (release 14; StataCorp LP).

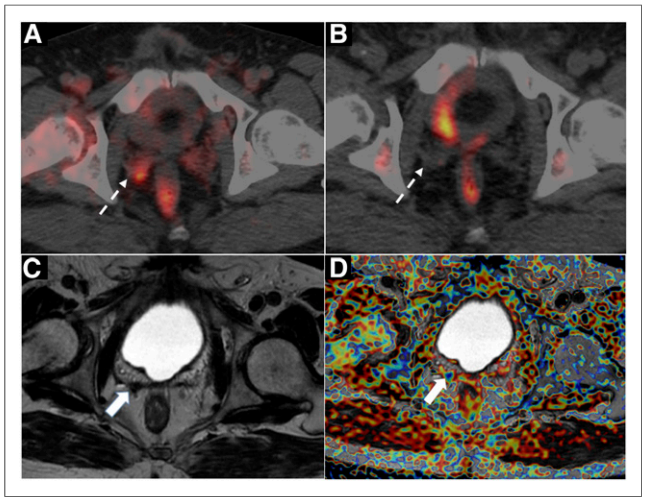

FIGURE 4. A 70-y-old man with Gleason 4 + 3 PCa treated with radical prostatectomy, with rising PSA level (1.34) and PSA doubling time of 5.3 mo. (A) $^{64}CuCl_2$ PET/CT images reveals focal uptake (dotted arrow) in residual right seminal vesicle. (B) ^{18}F-choline PET/CT is negative. (C) T2-weighted axial image mpMRI shows hypointense area in right seminal vesicle remnants. (D) Apparent-diffusion-coefficient map derived from diffusion-weighted imaging sequence shows focal area of signal restriction in correspondence to remnants of right seminal vesicle.

RESULTS

Adverse Events

No drug-related pharmacologic effects or physiologic responses occurred. No adverse reactions were observed after the injection of $^{64}CuCl_2$. All observed parameters (i.e., blood pressure, heart rate, body temperature) remained normal and unchanged during and after the examination. No patient reported subjective symptoms. In addition, no modification of the above-mentioned blood tests was reported 10 d after $^{64}CuCl_2$ injection.

Tracer Distribution and Dosimetry

Physiologic uptake of $^{64}CuCl_2$ differed from that of ^{18}F-choline. ^{64}CuCl showed high uptake in the liver and less intense uptake in the salivary glands, biliary tract, pancreas, spleen, and kidney. No significant ^{64}CuCl uptake was found in the bone marrow. ^{64}CuCl was not excreted via the urinary tract, and no accumulation in the bladder was found (Fig. 1).

The critical organ for ^{64}CuCl is the liver, as was already reported in ICRP 53 (*29*) and in a study by Capasso et al. (*12*). The liver accumulates about 30% of the administered activity, and the absorbed dose is 2.71E−1 mGy/MBq. Table 2 shows the absorbed dose per administered activity and comparison with ^{18}F-choline and ^{68}Ga-PSMA. Uptake in the liver, pancreas, and gallbladder maximizes about 1.5–2 h after administration, whereas the kidneys, spleen, and salivary glands have rapid uptake, maximizing in less than 1 h. Supplemental Figure 1 (supplemental materials are available at http://jnm.snmjournals.org) shows typical time–activity curves (as percentages of the injected activity) for the various source organs. Radiation dosimetry revealed an effective dose of 2.83E−2 mSv/MBq.

Lesion Kinetics

As in the case of organs at risk, time–activity curves for lesions showed rapid uptake, maximizing about 1 h after administration (Supplemental Fig. 2). The study of the lesion time–activity curves revealed a slow clearance dictated by the radionuclide physical half-life (mean effective half-life, 9.5 h).

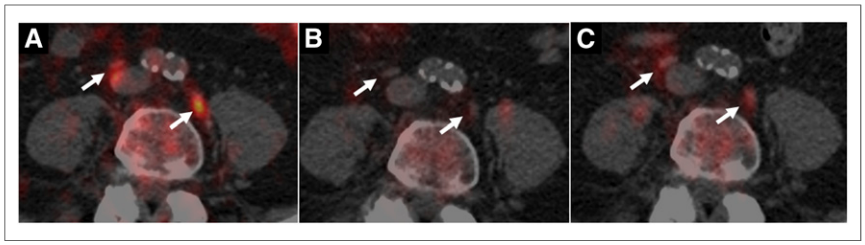

FIGURE 5. An 81-y-old man with Gleason 5 + 4 PCa treated with EBRT, with rising PSA level (1.09) and PSA doubling time of 4.9 mo. (A) $^{64}CuCl_2$ PET/CT images reveal 2 positive small iliac lymph nodes. (B) ^{18}F-choline PET/CT is negative (arrows). (C) Four months later (PSA value, 3.1), ^{18}F-choline PET/CT reveals correspondence between positive uptake and 2 iliac lymph-nodes (arrows).

Patient-Based Analysis

PCa relapse was found in 44 patients. Local relapse was detected in 34 patients (68%). We identified lymph node metastases in 17 patients (34%) and bone metastases in 5 patients (10%).

Table 3 summarizes the differences in DR between $^{64}CuCl_2$ PET/CT and each of the other 4 diagnostic modalities and shows the DRs recorded when different sites of PCa recurrence were considered separately. The difference between the DR of $^{64}CuCl_2$ PET/CT and that of ^{18}F-choline PET/CT was statistically significant ($P = 0.002$).

When the level of PSA was considered (Fig. 2), $^{64}CuCl_2$ PET/CT identified a higher number of positive patients than did ^{18}F-choline PET/CT in every PSA level cohort, except for a PSA level of more than 4 ng/mL.

When we considered the differences between the prostatectomy and nonprostatectomy populations, we found that $^{64}CuCl_2$ PET/CT identified a higher number of positive patients than did ^{18}F-choline PET/CT among those treated with surgery ($P = 0.001$). In particular, $^{64}CuCl_2$ PET/CT identified a significantly higher number ($P < 0.001$) of local relapses (Supplemental Table 1).

A detailed description of the multidisciplinary standard of reference considered for each patient is provided in Supplemental Figure 3.

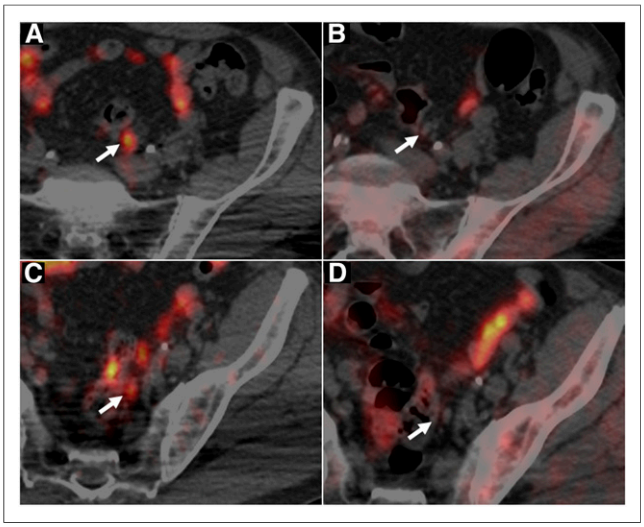

FIGURE 6. A 62-y-old man with Gleason 4 + 3 PCa treated with radical prostatectomy, with rising PSA level (1.32) and PSA doubling time of 3.7 mo. (A and C) $^{64}CuCl_2$ PET/CT images reveal 2 positive small left iliac lymph nodes. (B and D) ^{18}F-choline PET/CT is negative (arrows).

Lesion-Based Analysis

To determine the DR of each modality in detecting recurrent lesions in different anatomic locations, we also performed a lesion-based analysis; the results are summarized in Table 4. Overall, 118 lesions were detected in our analysis, 44 of which were local relapses, 60 abdominal lymph-node metastases, and 14 bone metastases (pelvis, proximal femurs, and lumbar spine). Indeed, $^{64}CuCl_2$ PET/CT showed significantly higher DRs than did ^{18}F-choline PET/CT and mpMRI (Table 4). The DR of $^{64}CuCl_2$ PET/CT was particularly high in the case of local relapse. Two cases of local recurrence are illustrated in Figures 3 and 4. In addition, $^{64}CuCl_2$ PET/CT identified a significantly higher number of lymph node metastases than did ^{18}F-choline PET/CT and mpMRI. In particular, all lymph nodes with positive $^{64}CuCl_2$ and negative ^{18}F-choline findings had a short-axis diameter of less than 7 mm. Two cases are illustrated in Figures 5 and 6. In the event of bone metastases, mpMRI showed the highest DR. No difference in bone DR was observed between ^{18}F-choline PET/CT and $^{64}CuCl_2$ PET/CT (Fig. 7).

All ^{18}F-choline-positive PCa lesions (local, lymph nodes, and bone) showed $^{64}CuCl_2$ uptake.

More generally, the $^{64}CuCl_2$ TBR evaluated 1 h after tracer injection was higher than that of ^{18}F-choline. The mean TBR was 13.4 for ^{18}F-choline and 16.4 for $^{64}CuCl_2$ ($P = 0.02$). The typical time–activity curves of $^{64}CuCl_2$ for fat, marrow, and muscles compared with that of one site of disease is illustrated in Supplemental Figure 4.

DISCUSSION

Our study was the first to prospectively evaluate the biodistribution, dosimetry, and lesion kinetics of $^{64}CuCl_2$ in a considerable number of PCa patients with biochemical relapse.

We found that the biodistribution of $^{64}CuCl_2$ was more suitable than that of ^{18}F-choline in evaluating PCa relapse, as $^{64}CuCl_2$ is neither excreted nor accumulated in the urinary tract. This enables better assessment of the pelvis and prostatic fossa, thus increasing the possibility of identifying small lesions close to the bladder or vesicourethral anastomosis.

We found that the critical organ for $^{64}CuCl_2$ was the liver, and we showed that the effective dose and liver exposure were lower than those calculated previously in only 7 patients (11% less and 8% less, respectively) (*12*). Our findings imply that potential hepatic radiotoxicity might be induced only by means of a high injected activity. We also found that the effective dose of $^{64}CuCl_2$ was about 40% greater than that of ^{18}F-choline (*30*). Thus, for an administered activity of 200 MBq, the effective dose of ^{64}CuCl is 5.7 mSv, whereas that of ^{18}F-choline is 4 mSv (*30*). However, this difference in radiation exposure can be considered negligible, especially in elderly patients with PCa biochemical relapse.

The time–activity curves of the PCa site of disease showed that $^{64}CuCl_2$ has a rapid uptake that maximizes about 1 h after administration. This result supports the choice to perform PET imaging early after the injection. In addition, this analysis showed that the $^{64}CuCl_2$ clearance in PCa relapse is slow and dictated by the radionuclide physical decay.

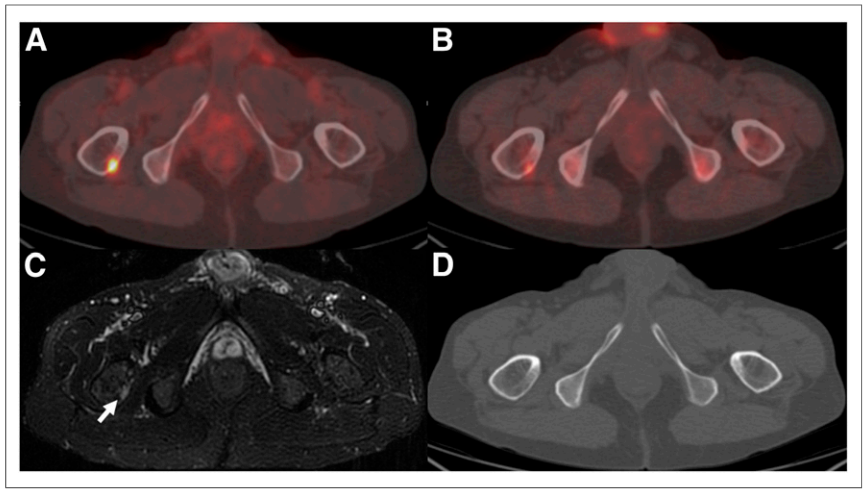

FIGURE 7. A 79-y-old man with Gleason 4 + 5 PCa treated with radical prostatectomy, with rising PSA level (1.89) and PSA doubling time of 2.1 mo. Both $^{64}CuCl_2$ PET/CT and ^{18}F-choline PET/CT images reveal intense, focal tracer uptake in proximal epiphysis of right femur. However, TBR was higher for $^{64}CuCl_2$ PET/CT than for ^{18}F-choline PET/CT (24.2 vs. 7.8). (C and C) Bone lesion (arrow) is evident on short T1 inversion recovery image (C) but is not appreciable in corresponding axial CT image (D).

These data on dosimetry, biodistribution, and kinetics are potentially useful. Indeed, given its decay scheme (half-life, 12.7 h; β^+, 17.86%; β^-, 39.0%) (*31*), ^{64}Cu could play a dual role in the development of molecular agents for PET imaging and in oncologic therapy (*32*). The additional emission of Auger electrons associated with the electron capture decay canal (electron capture, 43.075%) might considerably contribute to the possible therapeutic effectiveness of this radionuclide. Auger electrons have low kinetic energies and short-range penetration but concomitantly high linear-energy transfer (*33*), like heavier particles (*34,35*). The present study might provide the basis for evaluating the radiation safety of $^{64}CuCl_2$ and estimating the dose absorbed by organs at risk in the case of theranostic application.

Our study demonstrated that $^{64}CuCl_2$ PET/CT could detect local recurrence and lymph node and bone metastases in PCa patients with biochemical relapse and was the first to prospectively compare the diagnostic performance of $^{64}CuCl_2$ PET/CT with those of ^{18}F-choline PET/CT and mpMRI.

In our patient-based analysis, the DR of $^{64}CuCl_2$ PET/CT was significantly higher than that of ^{18}F-choline PET/CT. This difference stems from the high DR of $^{64}CuCl_2$ PET/CT in identifying local recurrence, which is often undetected by ^{18}F-choline PET/CT. In this analysis, no difference emerged between $^{64}CuCl_2$ PET/CT and mpMRI. This is in line with the well-known high sensitivity of mpMRI in detecting local recurrence (*36*).

Indeed, $^{64}CuCl_2$ PET/CT detected more patients with PCa relapse than did ^{18}F-choline PET/CT in each PSA cohort, except for a PSA level of more than 4 ng/mL. These data demonstrate the high DR of $^{64}CuCl_2$ PET/CT even in patients with a PSA level of less than 1 ng/mL. In this subgroup, more than 70% of patients presented a positive $^{64}CuCl_2$ PET/CT, which was often consistent with local relapse. In other words, these patients may still benefit from salvage, PET-guided RT (*37*).

In the lesion-based analysis, $^{64}CuCl_2$ PET/CT had a significantly higher DR than did ^{18}F-choline PET/CT and mpMRI. We found that the significant difference in DR was due to the greater ability of $^{64}CuCl_2$ PET/CT to detect both local recurrence and lymph node metastases (especially in small lymph nodes; i.e., those with a short axis diameter of $<$7 mm).

These findings open a door to the possibility of using $^{64}CuCl_2$ PET/CT in cases of suspected local PCa relapse when mpMRI remains inconclusive.

Despite our encouraging results, some important limitations should be noted. First, we assessed only the DRs of the diagnostic techniques mentioned, assuming a priori that all patients were true-positives, in that they presented with biochemical relapse. Indeed, we introduced a descriptive standard of reference, which was used only to confirm the sites of disease without providing information on the diagnostic accuracy of $^{64}CuCl_2$ PET/CT. Second, only a few cases of local findings were confirmed histopathologically. Histopathology was performed on transrectal ultrasound–guided biopsy in 7 of 25 patients (28%) showing only local recurrence; this confirmed the presence of disease. In addition, undetectable PSA values were found after salvage EBRT in another 4 of the 11 patients with only local recurrence and not previously treated with EBRT. Generally, we found a high concordance between positive findings on $^{64}CuCl_2$ PET/CT, ^{18}F-choline PET/CT, and mpMRI.

However, the lack of proper histopathologic confirmation is common in most articles (*16–19,38*) comparing different PET tracers in the detection of PCa recurrence. Indeed, the aim of these studies, as in our case, was not to determine the diagnostic accuracy but to assess and compare the DRs of the tracers.

CONCLUSION

The biodistribution of $^{64}CuCl_2$ is more suitable than that of ^{18}F-choline for exploring the pelvis and prostatic bed. The $^{64}CuCl_2$ effective dose is similar to those of other established PET tracers. In patients with biochemical relapse and a low PSA level, $^{64}CuCl_2$ PET/CT shows a significantly higher DR than does ^{18}F-choline PET/CT. Larger trials with this PET tracer are expected to further define its capabilities and role in the management of PCa.

DISCLOSURE

No potential conflict of interest relevant to this article was reported.

REFERENCES

1. Sproull M, Brechbiel M, Camphausen K. Antiangiogenic therapy through copper chelation. *Expert Opin Ther Targets.* 2003;7:405–409.
2. Raju KS, Alessandri G, Ziche M, Gullino PM. Ceruloplasmin, copper ions, and angiogenesis. *J Natl Cancer Inst.* 1982;69:1183–1188.
3. Ziche M, Jones J, Gullino PM. Role of prostaglandin E1 and copper in angiogenesis. *J Natl Cancer Inst.* 1982;69:475–482.
4. Hu GF. Copper stimulates proliferation of human endothelial cells under culture. *J Cell Biochem.* 1998;69:326–335.
5. Fuchs AG, Lustig ED. Localization of tissue copper in mouse mammary tumors. *Oncology.* 1989;46:183–187.

6. Canelas HM, DeJorge FB, Pereira WC, Sallum J. Biochemistry of cerebral tumours: sodium, potassium, calcium, phosphorus, magnesium, copper and sulphur contents of astrocytoma, medulloblastoma and glioblastoma multiforme. *J Neurochem.* 1968;15:1455–1461.
7. Kaiser J, Gullotta F. Estimation of the copper content of astrocytomas and glioblastomas by the cuproin method. *Neurochirurgia (Stuttg).* 1980;23:20–23.
8. Sparks R, Peng F. Positron emission tomography of altered copper metabolism for metabolic imaging and personalized therapy of prostate cancer. *J Radiol Radiat Ther.* 2013;1:1015.
9. Panichelli P, Villano C, Cistaro A, et al. Imaging of brain tumors with copper-64 chloride: early experience and results. *Cancer Biother Radiopharm.* 2016;31:159–167.
10. Peng F, Lu X, Janisse J, Muzik O, Shields AF. PET of human prostate cancer xenografts in mice with increased uptake of $^{64}CuCl_2$. *J Nucl Med.* 2006;47:1649–1652.
11. Cai H, Wu JS, Muzik O, Hsieh JT, Lee RJ, Peng F. Reduced ^{64}Cu uptake and tumor growth inhibition by knockdown of human copper transporter 1 in xenograft mouse model of prostate cancer. *J Nucl Med.* 2014;55:622–628.
12. Capasso E, Durzu S, Piras S, et al. Role of ^{64}CuCl 2 PET/CT in staging of prostate cancer. *Ann Nucl Med.* 2015;29:482–488.
13. Beheshti M, Haim S, Zakavi R, et al. Impact of ^{18}F-choline PET/CT in prostate cancer patients with biochemical recurrence: influence of androgen deprivation therapy and correlation with PSA kinetics. *J Nucl Med.* 2013;54:833–840.
14. Castellucci P, Fanti S. Prostate cancer: identifying sites of recurrence with choline-PET-CT imaging. *Nat Rev Urol.* 2015;12:134–135.
15. Mamede M, Ceci F, Castellucci P, et al. The role of ^{11}C-choline PET imaging in the early detection of recurrence in surgically treated prostate cancer patients with very low PSA level, 0.5 ng/mL. *Clin Nucl Med.* 2013;38:e342–e345.
16. Morigi JJ, Stricker PD, van Leeuwen PJ, et al. Prospective comparison of ^{18}F-fluoromethylcholine versus ^{68}Ga-PSMA PET/CT in prostate cancer patients who have rising PSA after curative treatment and are being considered for targeted therapy. *J Nucl Med.* 2015;56:1185–1190.
17. Schwenck J, Rempp H, Reischl G, Kruck S, Stenzl A, Nikolaou K. Comparison of ^{68}Ga-labelled PSMA-11 and ^{11}C-choline in the detection of prostate cancer metastases by PET/CT. *Eur J Nucl Med Mol Imaging.* 2017;44:92–101.
18. Nanni C, Schiavina R, Boschi S, Ambrosini V, Pettinato C, Brunocilla E. Comparison of ^{18}F-FACBC and ^{11}C-choline PET/CT in patients with radically treated prostate cancer and biochemical relapse: preliminary results. *Eur J Nucl Med Mol Imaging.* 2013;40(suppl 1):S11–S17.
19. Nanni C, Schiavina R, Brunocilla E, Boschi S, Borghesi M, Zanoni L. ^{18}F-fluciclovine PET/CT for the detection of prostate cancer relapse: a comparison to ^{11}C-choline PET/CT. *Clin Nucl Med.* 2015;40:e386–e391.
20. Piccardo A, Paparo F, Piccazzo R, et al. Value of fused ^{18}F-choline-PET/MRI to evaluate prostate cancer relapse in patients showing biochemical recurrence after EBRT: preliminary results. *BioMed Res Int.* 2014;2014:103718.
21. Paparo F, Piccardo A, Bacigalupo L, et al. Value of bimodal ^{18}F-choline-PET/MRI and trimodal ^{18}F-choline-PET/MRI/TRUS for the assessment of prostate cancer recurrence after radiation therapy and radical prostatectomy. *Abdom Imaging.* 2015;40:1772–1787.
22. Freitag MT, Radtke JP, Afshar-Oromieh A. Local recurrence of prostate cancer after radical prostatectomy is at risk to be missed in ^{68}Ga-PSMA-11-PET of PET/CT and PET/MRI: comparison with mpMRI integrated in simultaneous PET/MRI. *Eur J Nucl Med Mol Imaging.* 2017;44:776–787.
23. Cornford P, Bellmunt J, Bolla M, et al. EAU-ESTRO-SIOG guidelines on prostate cancer. Part II: treatment of relapsing, metastatic, and castration-resistant prostate cancer. *Eur Urol.* 2017;71:630–642.
24. Loevinger R, Berman M. *A Revised Schema for Calculating the Absorbed Dose from Biologically Distributed Radionuclides*: *MIRD Pamphlet no. I.* Reston, VA: Society of Nuclear Medicine and Molecular Imaging; 1976.
25. Snyder WS, Ford MR, Warner GG, Watson SBS. *Absorbed Dose per unit Cumulated Activity for Selected Radionuclides and Organs*: *MIRD Pamphlet No. 11.* Reston, VA: Society of Nuclear Medicine and Molecular Imaging, 1975.
26. Stabin MG, Sparks RB, Crowe E. OLINDA/EXM: The second-generation personal computer software for internal dose assessment in nuclear medicine. *J Nucl Med.* 2005;46:1023–1027.
27. 1990 Recommendations of the International Commission on Radiological Protection: ICRP publication 60. *Ann ICRP.* 1991;21.
28. The 2007 recommendations of the International Commission on Radiological Protection: ICRP publication 103. *Ann ICRP.* 2007;37:1–332.
29. Radiation dose to patients from radiopharmaceuticals: ICRP publication 53. *Ann ICRP.* 1988;18.
30. ICRP. Radiation dose to patients from radiopharmaceuticals: Addendum 3 to ICRP publication 53—ICRP publication 106. *Ann ICRP.* 2008;38:1–197.
31. Eckerman K, Endo A. ICRP publication 107. Nuclear decay data for dosimetric calculations. *Ann ICRP.* 2008;38:7–96.
32. Bryan JN, Jia JN, Mohsin F, et al. Monoclonal antibodies for copper-64 PET dosimetry and radioimmunotherapy. *Cancer Biol Ther.* 2011;11:1001–1007.
33. Howell RW. Radiation spectra for Auger-electron emitting radionuclides: report No. 2 of AAPM Nuclear Medicine Task Group No. 6. *Med Phys.* 1992;19:1371–1383.
34. Tavares AA, Tavares JM. ^{99m}Tc Auger electrons for targeted tumour therapy: a review. *Int J Radiat Biol.* 2010;86:261–270.
35. McMillan DD, Maeda J, Bell JJ, et al. Validation of ^{64}Cu-ATSM damaging DNA via high-LET Auger electron emission. *J Radiat Res (Tokyo).* 2015;56:784–791.
36. Barchetti F, Panebianco V. Multiparametric MRI for recurrent prostate cancer post radical prostatectomy and postradiation therapy. *BioMed Res Int.* 2014;2014:316272.
37. Tendulkar RD, Agrawal S, Gao T, et al. Contemporary update of a multi-institutional predictive nomogram for salvage radiotherapy after radical prostatectomy. *J Clin Oncol.* August 15, 2016 [Epub ahead of print].
38. Eiber M, Maurer T, Souvatzoglou M, et al. Evaluation of hybrid ^{68}Ga-PSMA ligand PET/CT in 248 patients with biochemical recurrence after radical prostatectomy. *J Nucl Med.* 2015;56:668–674.
39. Afshar-Oromieh A, Hetzheim H, Kübler W, et al. Radiation dosimetry of ^{68}Ga-PSMA-11 (HBED-CC) and preliminary evaluation of optimal imaging timing. *Eur J Nucl Med Mol Imaging.* 2016;43:1611–1620.